Animal Conservation

ZSL

Animal Conservation. Print ISSN 1367-9430

Comparing abundance estimates of a cryptic carnivore in southern Patagonia using two experimental methods

L. M. Elbroch[1], S. H. Williams[1], O. Ohrens[1], K. Pilgrim[2], A. Moeller[3], S. Arroyo-Arce[1], M. Parker[4], D. Goic[5], H. Robinson[1] & M. K. Schwartz[2]

1 Panthera, New York, New York, USA
2 USDA Forest Service, National Genomics Center for Wildlife and Fish Conservation, Rocky Mountain Research Station, Missoula, MT, USA
3 Wildlife Biology Program, Department of Ecosystem and Conservation Sciences, W.A. Franke College of Forestry and Conservation, University of Montana, Missoula, MT, USA
4 Working Dogs for Conservation, Missoula, MT, USA
5 La Leona Amarga Expeditions, Puerto Natales, Magallanes, Chile

Keywords
density; *Puma concolor*; SECR; Space-to-event; Torres del Paine; unmarked estimators.

Correspondence
L. Mark Elbroch, Panthera, 8 West 40th Street, 18th Floor, New York, NY 10018, USA.
Email: melbroch@panthera.org

Editor: Vincenzo Penteriani
Associate Editor: Nathan Hostetter

Code and data are archived in a public repository here: https://github.com/williash23/PT-Puma-Patagonia-Abundance.

Received 08 May 2023; accepted 30 September 2023

doi:10.1111/acv.12915

Abstract

Determining the abundance of cryptic carnivores is central to building successful conservation management to mitigate conflicts and support coexistence strategies. For these reasons, there is considerable investment in developing reliable, cost-effective tools for estimating the abundance of wildlife. Nevertheless, field-based comparisons of abundance methods remain uncommon, even while essential to refining methods and coming to consensus around best practices. Here, we compare two approaches still being tested in real-world application for an emblematic puma (*Puma concolor*) population in the Torres del Paine UNESCO Biosphere Reserve in southern Chile: (1) the unmarked estimator, space-to-event model (STE), which utilizes photographs gathered with camera traps, and (2) the genotype spatial partial identity model (gSPIM), which is an adaptation of the more established spatially explicit genetic capture-recapture method (SECR) based on genetic data extracted from scats collected in systematic surveys. We show the tremendous variation in resulting STE estimates depending upon the start time of the analysis and length of the sampling window, and showcase a refined iterative sampling approach in a Bayesian framework to both utilize the full camera data and to stabilize density estimates for a given sampling window. Across all sampling, estimates from the STE model ranged from 3.19 (1.6–5.1 representing 10th and 90th percentile of credible intervals) to 7.38 (3.3–11.6) independent pumas 100 km^{-2}. By comparison, our gSPIM model estimated 5.1 independent pumas 100 km^{-2} (excluding kittens) (with credible intervals of 2.2–10.3). Neither method was compared with any known density to determine their accuracy. Nevertheless, we provide initial density estimates to guide conservation strategies for wildlife agencies and local communities overseeing and hosting nascent puma tourism and livestock ranching, as well as guidelines for the use of these methods for any wildlife species.

Introduction

Determining the abundance of cryptic species is central to building successful conservation strategies, supporting management actions where species are held in public trust, and diffusing arguments and misconceptions among stakeholders advocating for changes in their abundance (Santini *et al.*, 2018; Amburgey *et al.*, 2021; Beausoleil *et al.*, 2021). This is especially true for cryptic carnivores, as perceptions about their abundance impact the public's perceptions of the risks and benefits of coexistence, and tolerance more broadly (Mitchell *et al.*, 2018; Murphy *et al.*, 2022). For these reasons and more, there has been a tremendous investment in developing reliable, cost-effective tools for estimating the abundance of wildlife (e.g. track counts, Balme, Hunter, & Slotow, 2009, Alibhai, Jewell, & Evans, 2020; telemetry studies, Beausoleil *et al.*, 2021; genetic mark-recapture using scat-detecting dogs, hair snares, or biopsy darts, Mumma

et al., 2015; spatially-explicit capture recapture with camera traps, Foster & Harmsen, 2012; motion-triggered cameras and facial-recognition software, Clapham *et al*., 2020). For animals with spots, stripes and other features that make them individually-identifiable, camera traps in conjunction with spatially explicit capture recapture (SECR) models are widely used (e.g. Tempa *et al*., 2019). When estimating the abundance of species that are difficult to identify as individuals from sighting or camera data, managers and researchers generally rely upon more expensive, and sometimes more invasive, genetic techniques to identify individuals (e.g. biopsy darts; Proffit *et al*., 2020) or marking individuals with telemetry devices to determine residency and spatial overlap with conspecifics (Cooley *et al*., 2009; Rinehart, Elbroch, & Wittmer, 2014; Beausoleil *et al*., 2021). However, several new camera-based models have been developed in recent years to address unmarked estimators in which animals are not identified as individuals (Rowcliffe *et al*., 2008; Moeller, Lukacs, & Horne, 2018; Nakashima, Fukasawa, & Samejima, 2018).

The accuracy and precision of unmarked estimators in estimating cryptic species abundance are still being debated and refined (Gilbert *et al*., 2020; Amburgey *et al*., 2021; Murphy *et al*., 2022). A second complication, however, is that these different methods estimate the abundance of different parts of a population, making comparisons across populations that much more difficult (Murphy *et al*., 2022). For example, when scats and genetic sampling are used to build SECR models, the estimate is for all animals, including dependent young. In contrast, intensive capture and telemetry data generally yield estimates for resident adults, and with some modification, all independent animals (Beausoleil *et al*., 2021).

Pumas (*Puma concolor*) are a cryptic carnivore difficult to identify to the individual level in camera trap images (Alexander & Gese, 2018). They are the most widely distributed terrestrial species in the Americas, and a species for which numerous methods of density estimation have been developed (see Murphy *et al*., 2022 for a review). Given their disproportionate roles in supporting biodiversity and ecological resilience (Barry *et al*., 2019; LaBarge *et al*., 2022), their controversial status as a species that competes with humans for ungulate prey and other resources (Elbroch *et al*., 2017; Beausoleil *et al*., 2021), and their fragile conservation status in many areas across their range (e.g. California, Benson *et al*., 2019; Argentina, Gallo *et al*., 2021), researchers and wildlife managers are still grappling with identifying the most reliable, cost-effective means of determining their abundance at scale.

In Patagonia, pumas also support a growing tourism industry (Tortato, Hoogesteijn, & Elbroch, 2020) that evidence suggests may be improving tolerance for the species in ranching communities (Ohrens *et al*., 2021). The iconic Torres del Paine National Park, and adjacent ranches of the Torres del Paine UNESCO Biosphere Reserve, in particular, are garnering a global reputation as the place to see wild pumas (e.g. Dynasties II, BBC 2022; Our National Parks; Netflix 2021), and to witness cryptic behaviors (e.g. Lagos *et al*., 2017; Cárdenas *et al*., 2021). Like elsewhere with other carnivores around the world, the lack of reliable abundance estimates for the region fuel ongoing debate over resolving puma-livestock conflict and potential human safety issues (Soto Volkart, 2006; Ojeda & Pérez, 2009; Rinehart, Elbroch, & Wittmer, 2014).

Here, we compare puma density estimates for the primary area hosting puma tourism in southern Chile generated by two approaches still being tested in real-world application: (1) the unmarked estimator, space-to-event model (Moeller, Lukacs, & Horne, 2018; Ausband *et al*., 2022) which utilizes photographs gathered with camera traps, and (2) the genotype spatial partial identity model (gSPIM) (Augustine *et al*., 2020), which is an adaptation of the more established spatially explicit genetic capture-recapture method (SECR) (Woods *et al*., 1999), based on genetic data extracted from scats collected in systematic surveys. Space-to-event models (STE) have been applied post hoc to ungulates, wolves and bycatch puma data collected during an elk study (Moeller, Lukacs, & Horne, 2018; Loonam *et al*., 2021a; Ausband *et al*., 2022), but never fully following the assumptions of the model (e.g. random camera placement). Importantly, STE estimates the abundance of independent units on the landscape, meaning that family units traveling closely together are counted as 1 (assuming sufficient intervals between sampling periods). In contrast, the genetic-based gSPIM method estimates the abundance of all pumas, including dependent kittens. In general, 33% of puma populations are dependent kittens (Murphy *et al*., 2022), and in any given area, females generally outnumber males by 2–3 times (Quigley & Hornocker, 2010). Therefore, we compared these two methods by applying a correction factor of 33% to the gSPIM estimate, to remove dependent kittens, following recommendations in Murphy *et al*. (2022). We close with guidance for the application of these methods in future wildlife studies.

Materials and methods

Study area

The Torres del Paine UNESCO Biosphere Reserve encompasses 770 889 ha, inclusive of private ranches and marine systems forming the Buffer zone. Our study area was the open steppe grassland habitat in the southern and eastern portions of Torres del Paine National Park, and adjacent private lands of Estancia Laguna Amarga and Estancia Lazo in Chilean Patagonia (Fig. 1). Puma tourism has occurred in the area to some degree for 20 years, but surged in growth beginning in 2014 adjacent the national park on private lands (Tortato, Hoogesteijn, & Elbroch, 2020). The landscape was Patagonia shrub-steppe, composed of xerophytic vegetation adapted to withstand drought and wind. Cushion shrubs and other short shrubs, including neneo *Mulinum spinosum*, calafate *Berberis heterophylla*, neo macho *Anarthrophyllum desideratum* and mata negra *Junellia tridens* were common, with tufted grasses between them. Precipitation occurs more commonly in winter from May to September, and totals 100–300 mm annually (Pisano, 1974).

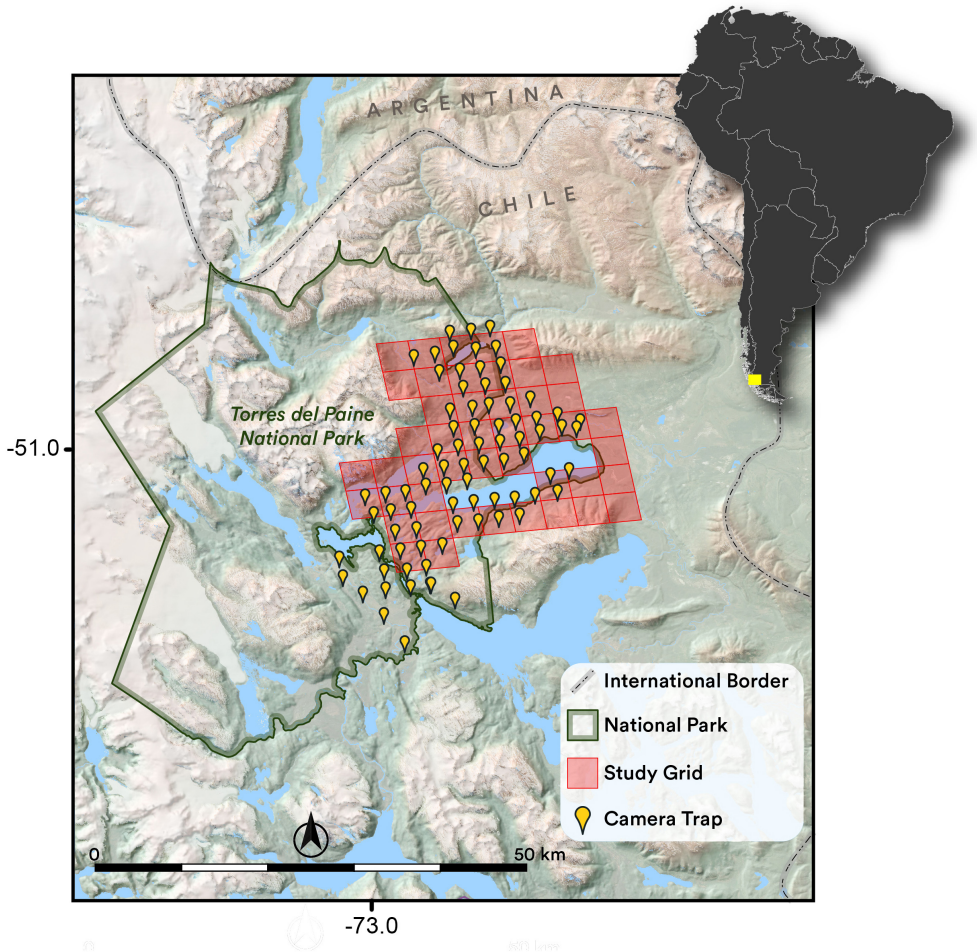

Figure 1 Study area in southern Chile, overlapping the eastern portions of Torres del Paine National Park. The yellow icons indicate the locations of the camera grid, and the squares are the sampling cells in which scat-detecting dogs and their handlers walked transects.

Abundance determined with cameras and space-to-event models

We deployed 80 motion-triggered cameras from May to September, 2019, and applied a space-to-event (STE) model to our data in the 'spaceNtime' package (Moeller & Lukacs, 2021) in R (ver. 4.2.0, R Core Team, 2022) to estimate the abundance of independent pumas in the study system (Moeller, Lukacs, & Horne, 2018). We chose not to use the similar time-to-event model due to the impact of animal speed on density estimates (Moeller, Lukacs, & Horne, 2018; Loonam *et al.*, 2021b) and our lack of movement parameters for this specific locale. We used V6 PantheraCams, which have a rapid response time of .08 s, a wide detection field captured with a 42° lens, and a short detection distance of 7 m, which resulted in viewsheds of 23.48 m^2 in the unobstructed habitat of this study system. We applied a 2.5-km point grid across our study system as a systematic process to ensure random sampling and then used handheld GPS units to navigate to these sites in the field (Fig. 1). Due to the open habitat, we were able to place cameras within 20 m of these points, only moving them slightly at times to provide some shelter from the wind to mitigate false triggers, or to ensure they were not plainly visible from a road or hiking trail.

STE leverages the time stamp on images collected from motion-triggered cameras to estimate animal abundance based on: (1) time-event analyses, (2) effort measured in unit space determined by measuring the viewshed of each camera in the field and (3) target species encounter rates:

$$\mathrm{STE} \sim \mathrm{Exp}(\lambda),$$

where STE is the amount of area (i.e. number of cameras) sampled before the target species is detected, drawn randomly without replacement at a single point in time, and λ is animals per camera viewshed in m^2. Animals detected within camera viewsheds are modeled following the Poisson distribution, and therefore the combined space (S) across camera viewsheds in the STE is modeled following an exponential distribution, $S \sim \mathrm{Exp}(\lambda)$ (Moeller, Lukacs, & Horne, 2018).

STE analysis assumes that the amount of area sampled in photographs (i.e. the combined viewsheds of cameras) until a target species is detected reflects effort, and that effort is inversely correlated with the species' density (Moeller, Lukacs, & Horne, 2018). The STE randomly samples active cameras across the grid, and the areas of their respective viewsheds, at a pre-determined time interval, here referred to as 'sampling frequency', to quantify how much space needs to be sampled (i.e. how many cameras) before the target species is detected. In other words, the higher the animal density, the more frequently the species is detected by cameras, the shorter the time intervals between detections, and ultimately the less space that needs to be sampled in an STE analysis until the target species is detected (Loonam *et al*., 2021a).

STE was originally conceptualized based on timelapse photos captured at predetermined intervals; however, it can be adapted to motion-triggered imagery in which photographs are captured only when a sensor detects motion. In the case of datasets collected by motion-triggered cameras, the data can be sampled to approximate a time lapse or instantaneous sampling in the 'spaceNtime' package (Moeller & Lukacs, 2021). When building sampling occasions and encounter histories for target species, researchers decide two critical parameters: (1) 'sampling frequency' or interval (i.e. the seconds between the start time of sampling occasions) (Fig. 2) and (2) the length of the 'sample window' (i.e. the duration of each sampling occasion in seconds) (Fig. 2). Increasing the sample window, for example, increases the opportunity for species detections at any point in time (Ausband *et al*., 2022).

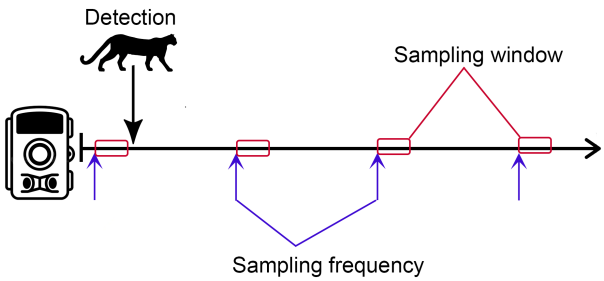

Figure 2 A conceptual illustration depicting a timeline at a single motion-triggered camera, inclusive of sampling frequency marked with blue arrows below the timeline, sampling windows illustrated by red rectangles on the timeline, and a single puma detection captured by the camera. The sampling frequency determines when the sampling window begins, and the length of the window is the total time recorded as a single sampling event. In this case, we miss detecting the puma given our start time, sampling frequency and sampling window. We could, however, lengthen our sampling window to increase detections, but this would also increase density estimates as well. We could also maintain the sampling frequency and sampling window, but shift the start time of our analyses, as we did here in our work. This allowed us to utilize the whole camera dataset and every puma detection, as well as simultaneously stabilized STE estimates.

Typically, a single dataset is generated for analysis using an arbitrary starting time (e.g. 08:00 h), a specified sampling frequency and a specified sample window length (Fig. 2). However, we were interested in exploring variation in density estimates generated from the same camera data partitioned differently, or more specifically: (1) samples obtained by changing the start time of sampling (which pulls a different subsample of photos from the complete dataset for analyses), and (2) changing the length of the sampling window, which others have indicated impacts density (Loonam *et al*., 2021b; Ausband *et al*., 2022). All our analyses utilized a 180 s sampling frequency (the length of time between sampling events) (Fig. 2).

First, for each given sampling frequency at 180 s, we generated every possible dataset from our camera data by shifting the start time of our analysis in 1-s increments (e.g. start times of 08:00 h, 08:00 h 01 s and 08:00 h 02 s; therefore, our sampling frequency of 180 s generated 180 unique datasets for density estimation). This allowed us to use all our puma detections and our complete camera data, and not just the subsample delineated by a specific start time, sampling window and sampling frequency. Second, for each of these datasets created by varying the start time, we also varied the length of the sample window from 2 to 10 s in 2-s intervals (2, 4, 6, 8, 10). Puma detections were binary (i.e. yes, no) regardless of the number of pumas detected at a camera station in a given sampling window, and the independence of detections was assumed given the distance between camera stations, which was far enough to ensure an individual puma could not be detected by multiple cameras in the same sampling window. We used the 'spaceNtime' package to generate an initial density estimate (animals/100 km^2). Then, we used this as an initial value within a Metropolis-Hastings MCMC algorithm to generate density estimates for all our datasets and sampling windows within a Bayesian framework. We used a large standard deviation (10) and normal distribution for the prior to avoid prior sensitivity. We ran each MCMC for 5000 iterations, discarded the first 1000 iterations as burn-in and retained the mean of the remaining iterations as the point estimate of density for each dataset.

Abundance determined with genotype spatial partial identity model

We divided our study system into 4 × 4 km quadrants, and in October–November, 2019, we sampled each with a single transect traveled by a trained scat-detecting dog (the handlers worked for Panthera and WorkingDogs4Conservation). Because of the practical constraints of terrain, transects varied in shape and length, resulting in different coverage of the 4 × 4 km cells. Once scats were identified by dogs in the field, handlers collected a 2-inch segment and stored it in a container with desiccant to dry the sample for storage and transport (Schwartz & Pilgrim, 2020). The location of the sample was recorded with a Garmin GPS unit and the characteristics of the site were gathered for future analyses.

Genetic analyses were conducted by the National Genomics Center for Wildlife and Fish Conservation in Missoula, Montana, USA. DNA from scat samples were analyzed using a panel of 19 microsatellite loci Fca08, Fca35, Fca43, Fca57, Fca77, Fca82, Fca90, Fca96, Fca132, Fca149, Fca176, Fca391, Fca559, LC109 (Culver *et al.*, 2000; Menotti-Raymond *et al.*, 2003), PcoA208, PcoB010, PcoB210, PcoC108 and PcoC112 (Kurushima *et al.*, 2006). DNA sex identification was performed using a field-specific sexing marker (Pilgrim *et al.*, 2005). We performed replicate genotyping in which each sample was PCR-amplified twice across the 19 variable microsatellite loci to screen for allele dropout, stutter artifacts and false alleles (DeWoody, Nason, & Hipkins, 2006). If any locus failed to amplify in either replicate or if there was a discrepancy in PCR amplification, the sample was repeated twice more to minimize genotyping error. If a genotype was confirmed by this repeat analysis, then it was retained. If a genotype failed again, the sample was assigned a missing score at the failed locus. After we removed any sample for which amplification failed at ≥one-third of loci, we screened remaining genotypes to detect and correct genotyping error using program DROPOUT 2.3 (McKelvey & Schwartz, 2005; Schwartz *et al.*, 2006).

Due to long delays in customs in combination with inadequate desiccant in sample tubes, the samples suffered significant genetic deterioration, limiting our ability to conduct a traditional SECR analysis. Therefore, we applied the genotype spatial partial identity model (gSPIM) (Augustine *et al.*, 2020), a hierarchical model with three sub-models, one for each of the ecological (spatial population), capture and genotype processes. The gSPIM integrates imperfect genetic individual identification (due to incomplete sequencing of genetic samples) with a spatial model built on assumptions of movement and home range heterogeneity within a Bayesian framework, that estimates the probability that paired scats are from the same individual based upon their proximity to each other.

We processed and formatted the input data according to the examples provided in Augustine *et al.* (2020) and made adjustments to account for effort as a function of the distance surveyed within each 4 × 4 km grid cell. Genetic sequencing of the targeted loci had between 2 and 9 possible alleles. Sequencing also determined sex for a number of samples and we included this information in the model (Male, Female, 0 for samples that could not be determined).

We ran the Poisson observation model version of the gSPIM using the R package 'nimble' (de Valpine *et al.*, 2017; de Valpine *et al.*, 2022, ver. 0.12.2) as developed by (Augustine *et al.*, 2020; using code provided by B. Augustine and available online at Augustine *et al.*, 2020; https://github.com/benaug/genotype-SPIM). We used the constant model for detection rate (i.e. no individual heterogeneity) and included a covariate for sample type, where a sample was considered high quality if the sample was identified to individual by geneticists and low quality otherwise. We ran the model for 3 chains at 300 000 iterations each and discarded the first 150 000 iterations as burn-in. We generated trace plots of MCMC chains and parameter estimates using the 'bayesplot' package (Gabry *et al.*, 2019, ver. 1.9.0.9000). We visually inspected trace plots and calculated the Gelman-Rubin statistic (Gelman & Rubin, 1992) to assess model convergence. We also provided a gSPIM-corrected estimate, or 33% less than our results, to estimate only independent pumas per 100 km^2, following recommendations made by Murphy *et al.* (2022). This allowed us to more directly compare our results with our STE estimates.

Results

Space-to-event

One camera was stolen during the project, and therefore we analyzed the photographs of 79 cameras which captured 102 independent puma events. Varying the start time produced a variety of density estimates for the same survey, but assessing the mean of this variation stabilized outputs considerably (Fig. 3); overall, the frequency of density estimates were skewed to the left (Fig. 4). Increasing the length of the sampling window decreased the space analyzed (i.e. the number of cameras counted) until the first puma detection and the number of overall datasets with zero puma detections (Table 1); it also increased puma density estimates in near linear fashion (Table 2; Fig. 3).

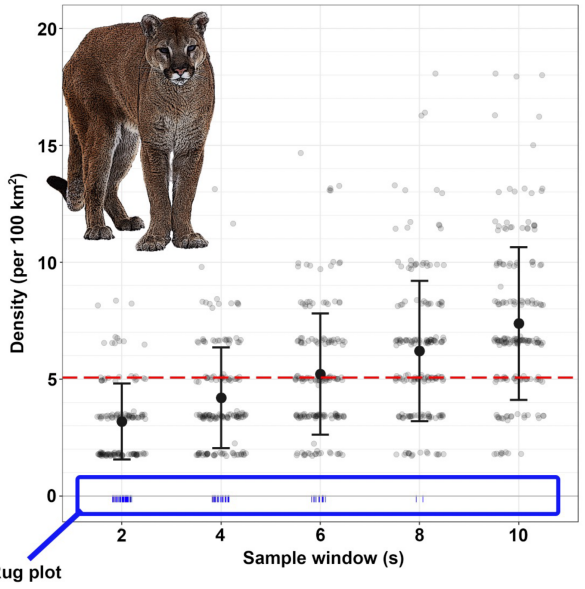

Figure 3 Density estimates (independent animals/100 km^2) generated from the STE model run via Bayesian implementation. Black points and error bars indicate means ±1 SD across all datasets generated within a given sample window. The dashed horizontal line is the mean density of independent pumas per 100 km^2 generated via our gSPIM analysis for comparison. The rug plot in blue is a visual representation of the number of data samples with zero puma detections for each sample window.

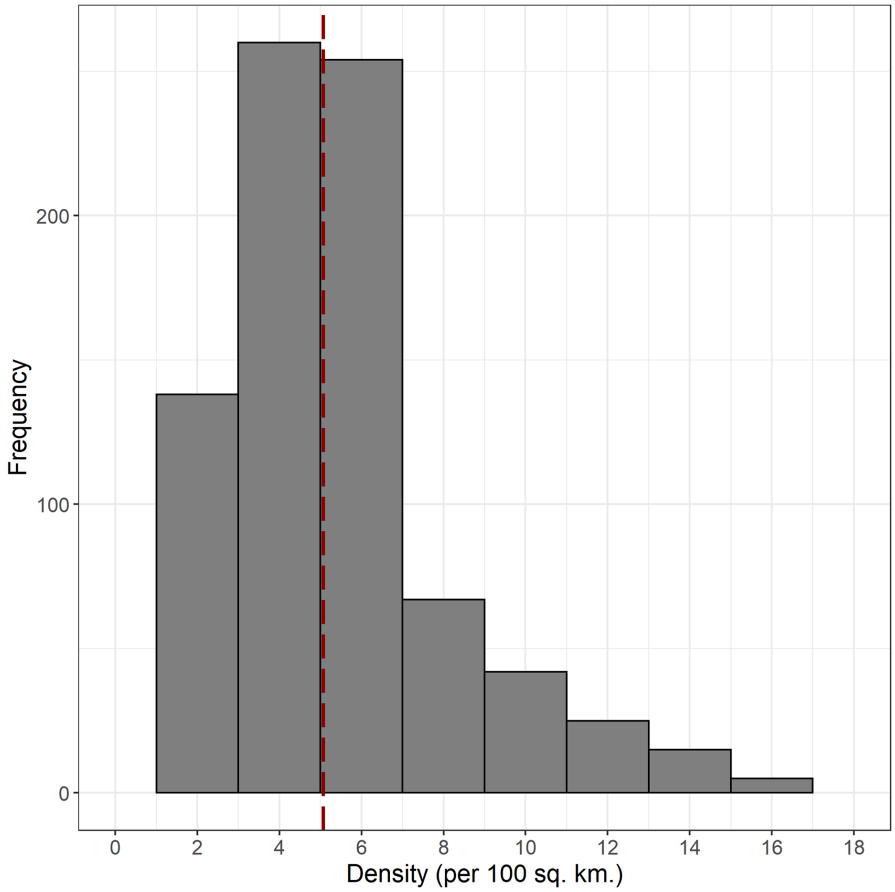

Figure 4 Histogram of all density estimates (independent animals/100 km^2) generated from the STE model run via Bayesian implementation across all sample windows. The dashed vertical line is the mean density of independent pumas per 100 km^2 generated via our gSPIM analysis for comparison.

Table 1 Number of detections from camera data, median number of occasions until first puma detection, and number of datasets with zero puma detections (and thus zero possible density estimates) across all datasets generated at each sample length

Sample length (s)	Number of puma detections range (mean, median)	Median number of occasions until first detection	Number of datasets with zero detections
2	0–5 (1.35, 1)	13 417	50
4	0–8 (2.13, 2)	12 342	26
6	0–9 (2.91, 3)	8314	12
8	0–11 (3.69, 3.5)	6716	2
10	1–11 (4.45, 4)	6293	0

Table 2 The mean, 10th percentile and 90th percentile puma densities (independent animals/100 km^2) across all datasets generated for each sample length

Sample length	Mean	10th percentile	90th percentile
2	3.19	1.63	5.10
4	4.20	2.16	6.70
6	5.21	2.60	8.30
8	6.20	3.00	9.92
10	7.38	3.27	11.59

Genotype spatial partial identity model

After discretizing, we had 32 grid cells that included transect effort, and each grid cell was sampled between 1 and 6 'occasions' based on the amount of surveyed transects that fell within each cell (median = 2). We gathered 385 scat samples in the field, and 96 scat samples were identified as puma. We were able to obtain DNA sex identification from 38 puma samples (40.0%) and we obtained individual identification from 23 of them (24%; Table S1). Direct-count repeat genotyping error rates per allele ranged from 0.00 to 0.027 across samples and loci. We identified 20 unique pumas (13 females and 7 males; Table S1), and of these, two females and one male were captured twice. An additional 19 samples yielded partial genotypes and were included in the model (Table S1).

Parameter estimates for home range scale (σ), baseline detection rate (λ_0) and individual inclusion probability (ψ)

Table 3 Results and summary statistics for the gSPIM model

	Median	Mean	SD	LCI	UCI
Density (total pumas/ 100 km^2)	7.102	7.567	3.025	3.259	15.344
Corrected density (independent pumas/ 100 km^2)	4.758	5.070	2.027	2.184	10.280
Num. of unique individuals captured	29	29	1.758	26	33
Baseline detection rate	0.095	0.103	0.049	0.032	0.221
Individual inclusion probability	0.340	0.367	0.148	0.156	0.745
Home range spatial scale	4.090	4.423	1.383	2.762	8.228

Mean and median total puma density and independent puma density estimates for the gSPIM model, and their associated standard deviations (SD), lower credible interval (LCI) and upper credible interval (UCI), followed by corrected mean and median puma abundance, number of unique individuals estimated by the model; and parameter estimates for baseline detection rate (λ_0), inclusion probability (ψ) and home range spatial scale (σ) in km.

are found in Table 3. The model estimated that 29 unique individuals were captured, which included nine additional individuals as compared to those with full genotype information (Table S1). Mean puma density estimated via gSPIM was 7.6 total pumas 100 km^{-2}, and after applying the correction factor of 33% to remove dependent young (Murphy *et al*., 2022), 5.1 independent pumas 100 km^{-2} (Table 3).

Discussion

We emphasize the experimental nature of both density estimates utilized in our study, and that neither are compared with any known density to determine their accuracy. Nevertheless, both methods produced estimates of independent puma density for an emblematic puma population in a UNESCO Biosphere Reserve that can be used to support local conservation. Torres del Paine National Park likely hosts among the highest puma densities anywhere in the Americas, which by these methods may be much higher than median densities for the species reported elsewhere in North and South America (Murphy *et al*., 2022).

The STE approach proposed in Moeller, Lukacs, & Horne (2018) is attractive for numerous reasons. It allows for estimates of unmarked animals, (i.e. species without individual identifiers like spots and stripes that represent a large proportion of the animal kingdom), and the required camera grid to gather the relevant data is relatively cheap and easy to install. Camera data also provide ancillary data, such as prey diversity, occupancy, activity patterns and more that can be used to answer additional conservation questions. Our analyses contribute to ongoing refinement of this model. Here, we provide novel methods that utilize a full camera survey (by sampling with different start times to create different datasets), and that stabilize density estimates produced by STE for a particular sampling window and frequency (by averaging across estimates produced at different start times).

Our exploration of the sampling window, however, yielded more ambiguous guidance for future implementation of the STE model. One of the fundamental assumptions of STE is random camera placement (Moeller, Lukacs, & Horne, 2018; Loonam *et al*., 2021b), yet some researchers have suggested we break this assumption in the field in order to increase detections of rare or cryptic species (Ausband *et al*., 2022). This seems unsatisfactory given that this introduces biases related to researcher experience and field skills, which in turn impacts detection rates. In previous research utilizing the similar time-to-event model, selecting camera sites that increased detections of target species nearly doubled estimated animal density as compared to estimates based on random placement (Loonam *et al*., 2021b). Others have suggested deploying larger camera grids for longer sampling in the field to increase detection of rare species (Loonam *et al*., 2021a). We suggest the better solution is to refine recommendations for the sampling window when applying STE to cryptic species; previous research has utilized sampling windows ranging from 30 s sampling for pumas (Loonam *et al*., 2021a) to 2 s for gray wolves (*Canis lupus*) (Ausband *et al*., 2022). Perhaps by comparing estimates at different sampling windows with a more reliable estimator, such as traditional SECR to provide a comparison of 'truth', researchers can still maintain random placement and begin to narrow down which sampling windows match best with the behaviors and characteristics of different species. Our gSPIM estimates, for example, overlapped credible intervals for our STE results for sample windows ranging 4–10 s, however, given that credible intervals also incorporate the best probability of a result, our corrected gSPIM estimates for the abundance of independent pumas best matched our STE outputs with a 6-s sampling window. Habitat features, however, may also play a role in selecting the ideal sampling window. STE assumes complete detection probability, and in open terrain, animals may detect cameras sooner and more often, thus altering their movement paths and biasing detections and density estimates low. If this is the case, one might have to determine habitat-specific sampling windows for rare species.

Our gSPIM estimates exhibited wide credible intervals due to low samples and low numbers of identified individuals, highlighting the importance of field protocols (e.g. scat dog training and performance, the observer's ability to discern scats so as to reward dogs for finding target species, and proper scat storage to protect genetic material). As telemetry studies grow in the region, the ecological variables of species residency and home range overlap in the model can be further refined. Nevertheless, the gSPIM approach holds great promise for utilizing data in which genetic material has deteriorated or in which a low percentage of samples yield individual-specific identification, without which, we would have unlikely been able to estimate abundance from our samples.

Field-based comparisons of abundance methods are uncommon, yet essential to refining methods and coming to

consensus around best practices. At this time, we cannot definitively describe puma abundance in the Torres del Paine UNESCO Biosphere Reserve, however, our results here and elsewhere (Elbroch *et al*., 2023) make clear that Torres del Paine National Park and the adjacent ranches with puma tourism support higher puma densities than other areas across the Americas (Murphy *et al*., 2022). Our STE estimates may also have been biased low, given that STE assumes complete detection probability. As described above, if a puma were to see a camera in open terrain, and divert its path to circumvent it, this would reduce detections and therefore density estimates. Future work can refine defensible metrics for the region, but in the meantime, we encourage conservation scientists and local wildlife officials to strategize on how best to manage the varied costs and benefits of an abundant, rebounding puma population, and its impacts on local communities hosting both tourism and livestock ranching (Ohrens *et al*., 2021).

Acknowledgments

We thank Jorge Portales, Juan and Tomislav Goic, and Michael Arcos and others with CONAF for permissions to access the National Park and private properties to conduct this research. We also thank Paul Lukacs for his assistance in creating Metropolis-Hastings algorithm code for Bayesian implementation of the STE, and Bryce Tipton and Jolene Strand for genetic laboratory assistance.

Author contributions

L. Mark Elbroch, **Hugh Robinson**, **Sara H. Williams** and **Omar Ohrens** conceived the ideas and designed methodology. **L. Mark Elbroch**, **Omar Ohrens**, **Stephanny Arroyo-Arce** and **Megan Parker** collected the data. **Sara H. Williams** and **Kristine Pilgrim** analyzed the data. **L. Mark Elbroch**, **Sara H. Williams** and **Hugh Robinson** led the writing of the manuscript. All authors contributed critically to the drafts and gave final approval for publication.

Funding information

This work was supported by the Summerlee Foundation, the Regina Bauer Frankenberg Foundation, and the Carroll Petrie Foundation.

Conflict of interest

The authors declare no conflicts of interest.

References

Alexander, P.D. & Gese, E.M. (2018). Identifying individual cougars (*Puma concolor*) in remote camera images – Implications for population estimates. *Wildl. Res.* **45**, 274–281.

Alibhai, S., Jewell, Z. & Evans, J. (2020). The challenge of monitoring elusive large carnivores: an accurate and cost-effective tool to identify and sex pumas (*Puma concolor*) from footprints. *PLoS One* **15**, e0242584.

Amburgey, S.M., Yackel Adams, A.A., Gardner, B., Hostetter, N.J., Siers, S.R., McClintock, B.T. & Converse, S.J. (2021). Evaluation of camera trap-based abundance estimators for unmarked populations. *Ecol. Appl.* **31**, e02410.

Augustine, B.C., Royle, J.A., Linden, D.W. & Fuller, A.K. (2020). Spatial proximity moderates genotype uncertainty in genetic tagging studies. *Proc. Natl. Acad. Sci. USA* **117**, 17903–17912.

Ausband, D.E., Lukacs, P.M., Hurley, M., Roberts, S., Strickfaden, K. & Moeller, A.K. (2022). Estimating wolf abundance from cameras. *Ecosphere* **13**, e3933.

Balme, G., Hunter, L.T.B. & Slotow, R. (2009). Evaluating methods for counting cryptic carnivores. *J. Wildl. Manage.* **73**, 433–441.

Barry, J.M., Elbroch, L.M., Aiello-Lammens, M.E., Sarno, R.J., Seelye, L., Kusler, A., Quigley, H.B. & Grigione, M.M. (2019). Pumas as ecosystem engineers: ungulate carcasses support beetle assemblages in the Greater Yellowstone Ecosystem. *Oecologia* **189**, 577–586.

Beausoleil, R.A., Welfelt, L.S., Keren, I.N., Kertson, B.N., Maletzke, B.T. & Koehler, G.M. (2021). Long-term evaluation of cougar density and application of risk analysis for harvest management. *J. Wildl. Manage.* **85**, 462–473.

Benson, J.F., Mahoney, P.J., Vickers, T.W., Sikich, J.A., Beier, P., Riley, S.P.D., Ernest, H.B. & Boyce, W.M. (2019). Extinction vortex dynamics of top predators isolated by urbanization. *Ecol. Appl.* **29**, e01868.

Cárdenas, J., Moraga, R., Montt, M. & Elbroch, L.M. (2021). Novel foraging by pumas on rhea eggs observed during predator tourism. IUCN/SSC Cat Specialist Group. *Cat News* **72**, 8–9.

Clapham, M., Miller, E., Nguyen, M. & Darimont, C.T. (2020). Automated facial recognition for wildlife that lack unique markings: a deep learning approach for brown bears. *Ecol. Evol.* **10**, 12883–12892.

Cooley, H.S., Wielgus, R.B., Koehler, G.M., Robinson, H.S. & Maletzke, B.T. (2009). Does hunting regulate cougar populations: a test of the compensatory mortality hypothesis. *Ecology* **90**, 2913–2921.

Culver, M., Johnson, W.E., Pecon-Slattery, J. & O'Brien, S.J. (2000). Genomic ancestry of the American puma (*Puma concolor*). *J. Hered.* **91**, 186–197.

de Valpine, P., Paciorek, C., Turek, D., Michaud, N., Anderson-Bergman, C., Obermeyer, F., Wehrhahn Cortes, C., Rodrìguez, A., Temple Lang, D. & Paganin, S. (2022). *NIMBLE user manual*. R Package Manual Version 0.12.3.

de Valpine, P., Turek, D., Paciorek, C.J., Anderson-Bergman, C., Lang, D.T. & Bodik, R. (2017). Programming with models: writing statistical algorithms for general model structures with NIMBLE. *J. Comput. Graph. Stat.* **26**, 403–413.

DeWoody, J., Nason, J.D. & Hipkins, V.D. (2006). Mitigating scoring errors in microsatellite data from wild populations. *Mol. Ecol. Notes* **6**, 951–957.

Elbroch, L.M., Feltner, J. & Quigley, H. (2017). Human-carnivore competition for antlered ungulates: do pumas select for bulls and bucks? *Wildl. Res.* **44**, 523–533.

Elbroch, L.M., Lagos, N., Cardenas, J., Goic, D., Moraga, R. & Ohrens, O. (2023). Tourism and human computers offer new tools to monitor Patagonia's top carnivore. *Sci. Total Environ.* **877**, 162916.

Foster, R.J. & Harmsen, B.J. (2012). A critique of density estimation from camera-trap data. *J. Wildl. Manage.* **76**, 224–236.

Gabry, J., Simpson, D., Vehtari, A., Betancourt, M. & Gelman, A. (2019). Visualization in Bayesian workflow. *J. R. Stat. Soc. A* **182**, 389–402.

Gallo, O., Castillo, D.F., Godinho, R., Mac Allister, M.E., Fernández, G.P., Failla, M. & Casanave, E.B. (2021). Molecular data reveal a structured puma (*Puma concolor*) population in northern Patagonia, Argentina. *Mamm. Biol* **101**, 653–663.

Gelman, A. & Rubin, D.B. (1992). Inference from iterative simulation using multiple sequences. *Statist. Sci.* **7**, 457–472.

Gilbert, N.A., Clare, J.D.J., Stenglein, J.L. & Zuckerberg, B. (2020). Abundance estimation of unmarked animals based on camera-trap data. *Conserv. Biol.* **00**, 1–12.

Kurushima, J.D., Collins, J.A., Well, J.A. & Ernest, H.B. (2006). Development of 21 microsatellite loci for puma (*Puma concolor*) ecology and forensics. *Mol. Ecol. Notes* **6**, 1260–1262.

LaBarge, L., Evans, M.J., Miller, J.R.B., Cannataro, G., Hunt, C., Flemming, E. & Elbroch, L.M. (2022). Pumas as ecological brokers: a review of their biotic relationships. *Mamm. Rev.* **52**, 360–376.

Lagos, N., Sepúlveda, C., Pino, R., Segura, B., Gerstle, J., Gamboa, F. & Muñoz-Donoso, C. (2017). Social behaviour of pumas in Torres del Paine National Park, Chile. IUCN/SSC Cat Specialist Group. *Cat News* **66**, 38–39.

Loonam, K.E., Ausband, D.E., Lukacs, P.M., Mitchell, M.S. & Robinson, H.S. (2021*a*). Estimating abundance of an unmarked, low-density species using cameras. *J. Wildl. Manage.* **85**, 87–96.

Loonam, K.E., Lukacs, P.M., Ausband, D.E., Mitchell, M.S. & Robinson, H.S. (2021*b*). Assessing the robustness of time-to-event models for estimating unmarked wildlife abundance using remote cameras. *Ecol. Appl.* **31**, e02388.

McKelvey, K.S. & Schwartz, M.K. (2005). DROPOUT: a program to identify problem loci and samples for noninvasive genetic samples in a capture-mark-recapture framework. *Mol. Ecol. Notes* **5**, 716–718.

Menotti-Raymond, M., David, V.A., Agarwala, R., Schaffer, A.A., Stephens, R., O'Brien, S.J. & Murphy, W.J. (2003). Radiation hybrid mapping of 304 novel microsatellites in the domestic cat genome. *Cytogenet. Genome Res.* **102**, 272–276.

Mitchell, M.S., Cooley, H., Gude, J.A., Kolbe, J., Nowak, J.J., Proffit, K.M., Sells, S.N. & Thompson, M. (2018). Distinguishing values from science indecision making: setting harvest quotas for mountain lions in Montana. *Wildl. Soc. Bull.* **42**, 13–21.

Moeller, A.K. & Lukacs, P.M. (2021). spaceNtime: an R package for estimating abundance of unmarked animals using camera-trap photographs. *Mamm. Biol.* **102**, 581–590.

Moeller, A.K., Lukacs, P.M. & Horne, J.S. (2018). Three novel methods to estimate abundance ofunmarked animals using remote cameras. *Ecosphere* **9**, e02331.

Mumma, M.A., Zieminski, C., Fuller, T.K., Mahoney, S.P. & Waits, L.P. (2015). Evaluating noninvasive genetic sampling techniques to estimate large carnivore abundance. *Mol. Ecol. Resour.* **15**, 1133–1144.

Murphy, S.M., Beausoleil, R.A., Stewart, H. & Cox, J.J. (2022). Review of puma density estimates reveals sources of bias and variation, and the need for standardization. *Glob. Ecol. Conserv.* **35**, e02109.

Nakashima, Y., Fukasawa, K. & Samejima, H. (2018). Estimating animal density without individual recognition using information derivable exclusively from camera traps. *J. Appl. Ecol.* **55**, 735–744.

Ohrens, O., Tortato, F., Hoogensteijn, R., Sarno, R., Quigley, H., Goic, D. & Elbroch, L.M. (2021). Predator tourism improves tolerance for puma, but may increase future conflict among ranchers in Chile. *Biol. Conserv.* **258**, 109150.

Ojeda, M. & Pérez, H. (2009). *La caza del puma*. MS thesis, University of Magallanes, Punta Arenas.

Pilgrim, K.L., McKelvey, K.S., Riddle, A.E. & Schwartz, M.K. (2005). Felid sex identification based on noninvasive genetic samples. *Mol. Ecol. Notes* **5**, 60–61.

Pisano, E. (1974). Estudio ecologico de la region continental sur del area andino-patagonica, II. Contribuci'on a la fitogeografía de la zona del Parque Nacional Torres del Paine. *An. Inst. Patagon.* **5**, 59–104.

Proffit, K.M., Garrott, R., Gude, J.A., Hebblewhite, M., Jimenez, B., Paterson, J.T. & Rotella, J. (2020). Integrated carnivore-ungulate management: a case study in west-Central Montana. *Wildl. Monogr.* **206**, 1–28.

Quigley, H. & Hornocker, M. (2010). Cougar population dynamics. In *Cougar: ecology and conservation*: 59–75. Hornocker, M. & Negri, S. (Eds). Chicago: University of Chicago Press.

Rinehart, K., Elbroch, L.M. & Wittmer, H.U. (2014). Common biases in density estimation based on home range overlap with reference to puma density estimates in Patagonia. *Wildl. Biol.* **20**, 19–26.

Rowcliffe, J.M., Field, J., Turvey, S.T. & Carbone, C. (2008). Estimating animal density using camera traps without the need for individual recognition. *J. Appl. Ecol.* **45**, 1228–1236.

Santini, L., Isaac, N.J.B., Maiorano, L., Ficetola, G.F., Huijbregts, M.A.J., Carbone, C. & Thuiller, W. (2018).

Global drivers of population density in terrestrial vertebrates. *Glob. Ecol. Biogeogr.* **27**, 968–979.
Schwartz, M. & Pilgrim, K. (2020). Protocols for collecting and storing DNA samples. https://www.fs.usda.gov/rmrs/sites/default/files/documents/NationalGenomicsCenter_RMRS%20Sample%20StorageProtocols_2020.pdf
Schwartz, M.K., Cushman, S.A., McKelvey, K.S., Hayden, J. & Engkjer, C. (2006). Detecting genotyping errors and describing American black bear movement in northern Idaho. *Ursus* **17**, 138–148.
Soto Volkart, N. (2006). *Impact on wildlife farming in Magallanes*. SAG Punta Arenas, Chile: Med. Vet. Enc. Reg. Renewable Natural Resources.
Tempa, T., Hebblewhite, M., Goldberg, J.F., Norbu, N., Wangchuk, T.R., Xiao, W. & Mills, L.S. (2019). The spatial distribution and population density of tigers in mountainous terrain of Bhutan. *Biol. Conserv.* **238**, 108192.
Tortato, F., Hoogesteijn, R. & Elbroch, L.M. (2020). Have natural disasters created opportunities to initiate Big Cat Tourism in South America? *Biotropica* **52**, 400–403.
Woods, J.G., Paetkau, D., Lewis, D., McLellan, B.N., Proctor, M. & Strobeck, C. (1999). Genetic tagging of free-ranging black and brown bears. *Wildl. Soc. Bull.* **27**, 616–627.

Supporting information

Additional supporting information may be found online in the Supporting Information section at the end of the article.

Table S1. DNA results from puma scat samples. Individuals represented by more than one sample are shaded.
Table S2. All genotypes included in our gSPIM model.